Distributionally Robust Scheduling for Benefit Allocation in Regional Integrated Energy System with Multiple Stakeholders

Qinglin Meng, Xiaolong Jin, Fengzhang Luo, Zhongguan Wang, and Sheharyar Hussain

***Abstract*—A distributionally robust scheduling strategy is proposed to address the complex benefit allocation problem in regional integrated energy systems (RIESs) with multiple stakeholders. A two-level Stackelberg game model is established, with the RIES operator as the leader and the users as the followers. It considers the interests of the RIES operator and demand response users in energy trading. The leader optimizes time-of-use (TOU) energy prices to minimize costs while users formulate response plans based on prices. A two-stage distributionally robust game model with comprehensive norm constraints, which encompasses the two-level Stackelberg game model in the day-ahead scheduling stage, is constructed to manage wind power uncertainty. Karush-Kuhn-Tucker (KKT) conditions transform the two-level Stackelberg game model into a single-level robust optimization model, which is then solved using column and constraint generation (C&CG). Numerical results demonstrate the effectiveness of the proposed strategy in balancing stakeholders' interests and mitigating wind power risks.**

***Index Terms*—Regional integrated energy system (RIES), distributionally robust, Stackelberg game, uncertainty, demand response.**

I. Introduction

DRIVEN by the continuous advancement of Energy Internet policies, there has been a notable rise in integrated energy systems coupled with other networks, particularly the natural gas network, centered around the power grid, paving the way for a fresh development trend [1]-[3]. The regional integrated energy systems (RIESs) serve as a platform for amalgamating diverse user loads, energy conversion equipment, energy storage units, and distributed power sources. Its main objective is to accomplish harmonized planning, optimized operations, collaborative management, interactive response, and synergistic integration among various heterogeneous energy subsystems [4]-[6]. Concurrently, the evolution of energy markets has transformed users into active market participants, fostering intense competition and forming distinct interest groups. This emerging scenario has brought attention to the concept of source-load cooperation within the RIES, aiming to achieve optimal operations tailored to the preferences of different interest groups.

Numerous studies have been dedicated to optimizing the operation of RIESs. For instance, [7] proposed an economic scheduling model that considers power exchange among combined cooling heating and power (CCHP)-type multi-microgrids, improving system efficiency. Meanwhile, [8] employed a non-dominated sorting genetic algorithm-II for multi-objective optimization of a solar-compressed air energy storage-based combined heat and power (CHP) system, considering investment cost and energy efficiency. These studies, however, primarily emphasized supply-side optimization and overlooked the autonomous demand-side response behaviors and the interactions between stakeholders. To address this, Stackelberg's theory is utilized to coordinate multiple stakeholders' interests by balancing decision variables between upper-level and lower-level decision-makers. For instance, [9] introduced a comprehensive demand response (CDR) scheme for smart energy hubs, employing a Stackelberg game to reduce RIES operating costs. In the microgrid (MG) system with CHP generation, [10] used the Stackelberg game model to simulate the trading process between MG operators and users, thereby achieving optimized energy management in the system. Additionally, [11] introduced an energy management framework for a multi-energy industrial park based on the Stackelberg game, which considers the interactive mechanism between supply and demand. In this approach, the power supply side is considered as the leader, while the users are considered as the followers. It aims to achieve the coordinated interaction between supply and demand while maximizing the interests of both parties. Howev-

Manuscript received: September 11, 2023; revised: December 26, 2023; accepted: April 16, 2024. Date of CrossCheck: April 16, 2024. Date of online publication: May 29, 2024.

This work was supported by National Natural Science Foundation of China (No. 52207133) and Science and Technology Project of State Grid Corporation of China (No. 5400-202112571A-0-5-SF).

Q. Meng (corresponding author) is with the Comprehensive Service Center, State Grid Tianjin Electric Power Company, Tianjin 300010, China, and he is also with the Key Laboratory of Smart Grid of Ministry of Education, School of Electrical and Information Engineering, Tianjin University, Tianjin 300072, China, the School of Electrical Engineering, Tiangong University, Tianjin 300387, China, and the Key Laboratory of Smart Energy & Information Technology of Tianjin Municipality, Tianjin 300072, China (e-mail: qinglin.meng@ieee.org).

X. Jin, F. Luo, and Z. Wang are with the Key Laboratory of Smart Grid of Ministry of Education, School of Electrical and Information Engineering, Tianjin University, Tianjin 300072, China (e-mail: xljin@tju. edu. cn; luofengzhang@tju.edu.cn; wang_zg@tju.edu.cn).

S. Hussain is with the Institute of Marine Electronic and Intelligent System, Ocean College, Zhejiang University, Zhoushan, China (e-mail: ee.sbangash@zju.edu.cn).

DOI: 10.35833/MPCE.2023.000661

er, these studies did not account for the impact of wind power output uncertainty on formulating Stackelberg strategies.

Given the significant impact of intermittent and stochastic renewable energy output on stable RIES operation, addressing uncertainty in RIES scheduling has become increasingly vital. Currently, robust optimization and stochastic programming are two commonly used methods for modeling uncertainties. On the one hand, Robust optimization aims to find optimal solutions by considering worst-case scenarios but often exhibits inherent conservatism [12] - [14]. On the other hand, stochastic programming relies on accurate probability density distributions of uncertain variables, which can be challenging to obtain [15] - [17]. To overcome these limitations and leverage the advantages of both methods, distributionally robust optimization has emerged as a novel method gaining widespread attention. Reference [18] utilized 1-norm and ∞-norm constraints on fuzzy sets of scene probability distributions to effectively avoid issues, including non-deterministic polynomials, in the process of identifying the optimal decision variables under the most adverse probabilistic conditions within discrete scenarios. Reference [19] developed a fuzzy set for wind power uncertainty based on the Wasserstein distance. Building on this, a data-driven RIES scheduling model was proposed to ensure that the scheduling outcomes are insensitive and robust to probability density function perturbations. Furthermore, [20] improved this method by integrating the Wasserstein distance with kernel density estimation, resulting in a more compact and reliable fuzzy set. This integration more effectively balances economic efficiency and robustness. Although distributionally robust optimization has been employed in RIES scheduling, the combination of Stackelberg game theory with distributionally robust optimization remains a relatively unexplored area with a paucity of studies.

This paper aims to address the limitations of previous studies by proposing a novel strategy that combines distributionally robust optimization and Stackelberg game theory for optimal scheduling in RIESs. First, a two-level leader-follower game model is established, in which RIES operators and CDR users are viewed as the leaders and followers, with time-of-use (TOU) energy pricing serving as the linkage between them. The objective of the leader is to minimize operational costs by determining optimal time-varying electricity prices, while the users formulate demand response plans based on these prices and their aggregated utility functions. Secondly, decision-making models for each gaming entity are constructed, incorporating a two-stage distributionally robust game model (TSDRGM) to address the uncertainty inherent in wind energy. Furthermore, a comprehensive norm constraint is introduced to mitigate the shortcomings of conservative robust optimization and the poor resistance of stochastic optimization. The follower model is treated as an equilibrium constraint to simplify the resolution process and is incorporated into the decision-making model of the leader using the Karush-Kuhn-Tucker (KKT) condition. This modification transforms the original two-level Stackelberg game model into a single-level sub-Brue-bar optimization model, which can be solved iteratively using the column and constraint generation (C&CG) algorithm. Finally, the effectiveness of the two-level Stackelberg game model is validated through simulation examples, providing evidence of its efficacy in addressing the challenges of optimal scheduling in RIESs.

II. Structure and Mathematical Model of RIES

A. Structure of RIES

RIES serves as a pivotal enabler for implementing concepts like multi-energy complementarity and optimizing energy efficiency. In the RIES framework described within this study, the electricity demand of the load is met by the main grid, wind turbines (WTs), and gas turbines (GTs). Gas boilers (GBs) and GTs also cater to the heat demand. A portion of the gas supplied by the gas network is directed towards the GT, while another portion is allocated to the GB. Cloud energy storage systems (CESSs) are utilized as energy buffers to augment the stability and flexibility of the system, encompassing both the cloud electrical storage (CES) and cloud thermal storage (CTS). These systems play a critical role in balancing and managing energy resources dynamically, enhancing the system stability and flexibility. On the load side, CDR is considered, allowing for load time-shifting and interruption capabilities. The specific energy coupling configuration is visually represented in Fig. 1.

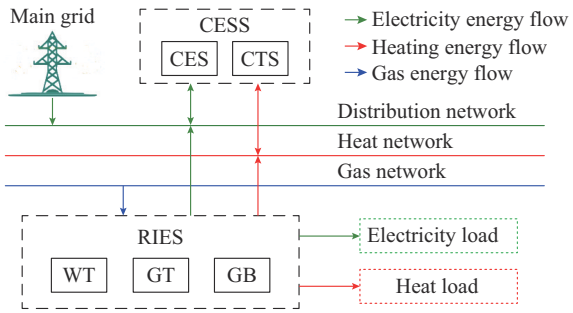

Fig. 1. Specific energy coupling configuration.

B. Electric-thermal Cogeneration Model

1) GT generates both electricity and heat through the combustion of natural gas. The constraints and outputs associated with GTs are as follows:

$$\begin{cases} P_{\mathrm{GT}}^{t}=\eta_{\mathrm{GT}}G_{\mathrm{GT}}^{t} \\ H_{\mathrm{GT}}^{t}=\eta_{\mathrm{GT,h}}\left(1-\eta_{\mathrm{GT}}\right)G_{\mathrm{GT}}^{t} \\ U_{\mathrm{GT}}^{t}P_{\mathrm{GT}}^{t,\min}\le P_{\mathrm{GT}}^{t}\le U_{\mathrm{GT}}^{t}P_{\mathrm{GT}}^{t,\max} \\ U_{\mathrm{GT}}^{t}H_{\mathrm{GT}}^{t,\min}\le H_{\mathrm{GT}}^{t}\le U_{\mathrm{GT}}^{t}H_{\mathrm{GT}}^{t,\max} \end{cases} \tag{1}$$

where P_{GT}^{t} and H_{GT}^{t} are the power generation and heating power of GT at time t, respectively; G_{GT}^{t} is the gas consumption of GT at time t; η_{GT} and $\eta_{\mathrm{GT,h}}$ are the power generation efficiency and heating efficiency of GT, respectively; $P_{\mathrm{GT}}^{t,\max}$ and $P_{\mathrm{GT}}^{t,\min}$ are the maximum and minimum power generation values of GT at time t, respectively; $H_{\mathrm{GT}}^{t,\max}$ and $H_{\mathrm{GT}}^{t,\min}$ are the maximum and minimum heating power values of GT at time t, respectively; and U_{GT}^{t} is a binary variable of GT indicating the on/off state.

2) The GB produces heat by burning natural gas. The heating power output and constraints associated with the GB are

as follows:

$$\begin{cases} H_{\mathrm{GB}}^{t}=\eta_{\mathrm{GB}}G_{\mathrm{GB}}^{t} \\ H_{\mathrm{GB}}^{t,\min}\le H_{\mathrm{GB}}^{t}\le H_{\mathrm{GB}}^{t,\max} \end{cases} \tag{2}$$

where H_{GB}^{t} is the heating power of GB at time t; G_{GB}^{t} is the gas consumption of GB at time t; η_{GB} is the heating efficiency of GB; and $H_{\mathrm{GB}}^{t,\max}$ and $H_{\mathrm{GB}}^{t,\min}$ are the upper and lower limits of the heating power of GB, respectively.

C. CESS

The CESS leverages energy storage resources from numerous small- and medium-sized users. It employs a "shared energy storage" approach, which maximizes the complementary nature and economies of scale in energy storage behavior. This approach helps avoid charging and discharging disorderliness while reducing costs for users. The CESS described in this study primarily comprises two types of energy storage: CES and CHS. The pertinent constraints for CESS can be outlined as follows:

$$\begin{cases} \alpha_1 E_{\mathrm{CESS}}\le E_{\mathrm{CESS}}^{t}\le \alpha_2 E_{\mathrm{CESS}} \\ 0\le E_{\mathrm{CESS}}\le E_{\mathrm{CESS}}^{\max} \\ 0\le P_{\mathrm{CESS}}^{t,\mathrm{ch}}\le P_{\mathrm{CESS}}^{\mathrm{ch}}u_{\mathrm{CESS}}^{t,\mathrm{ch}} \\ 0\le P_{\mathrm{CESS}}^{\mathrm{ch}}\le P_{\mathrm{CESS}}^{\mathrm{ch,max}} \\ 0\le P_{\mathrm{CESS}}^{t,\mathrm{dis}}\le P_{\mathrm{CESS}}^{\mathrm{dis}}u_{\mathrm{CESS}}^{t,\mathrm{dis}} \\ 0\le P_{\mathrm{CESS}}^{\mathrm{dis}}\le P_{\mathrm{CESS}}^{\mathrm{dis,max}} \\ u_{\mathrm{CESS}}^{t,\mathrm{ch}}+u_{\mathrm{CESS}}^{t,\mathrm{dis}}\le 1 \\ E_{\mathrm{CESS}}^{24}=E_{\mathrm{CESS}}^{0} \\ E_{\mathrm{CESS}}^{t}-E_{\mathrm{CESS}}^{t-1}(1-\delta_{\mathrm{CESS}})=\eta_{\mathrm{CESS}}^{\mathrm{c}}P_{\mathrm{CESS}}^{t,\mathrm{ch}}-P_{\mathrm{CESS}}^{t,\mathrm{dis}}/\eta_{\mathrm{CESS}}^{\mathrm{d}} \end{cases} \tag{3}$$

where E_{CESS}^{t} is the capacity of CESS at time t; E_{CESS} is the rented energy storage capacity of CESS; α_1 and α_2 are the upper and lower limits of the charging state of CESS, respectively; $E_{\mathrm{CESS}}^{\max}$ is the maximum capacity of CESS that can be rented; $P_{\mathrm{CESS}}^{t,\mathrm{ch}}$ and $P_{\mathrm{CESS}}^{t,\mathrm{dis}}$ are the charging and discharging power of CESS at time t, respectively; $P_{\mathrm{CESS}}^{\mathrm{ch}}$ and $P_{\mathrm{CESS}}^{\mathrm{dis}}$ are the charging and discharging power limits for rented CESS, respectively; $u_{\mathrm{CESS}}^{t,\mathrm{ch}}$ and $u_{\mathrm{CESS}}^{t,\mathrm{dis}}$ are the binary variables indicating the charging or discharging state of CESS, respectively; $P_{\mathrm{CESS}}^{\mathrm{ch,max}}$ and $P_{\mathrm{CESS}}^{\mathrm{dis,max}}$ are the upper limits of charging and discharging power for rented CESS, respectively; $\eta_{\mathrm{CESS}}^{\mathrm{c}}$ and $\eta_{\mathrm{CESS}}^{\mathrm{d}}$ are the charging and discharging efficiencies of CESS, respectively; and δ_{CESS} is the self-loss coefficient of CESS.

D. CDR

In this study, the electricity load is categorized into two main types: fixed load and flexible load. The flexible load is further subdivided into two distinct types based on their demand response characteristics: shiftable load (SL) and interruptible load (IL).

SL: it refers to a type of electricity consumption where the total amount of electricity remains constant, but the timing of consumption can be flexibly adjusted [21]. The characteristics of SL can be described as:

$$\begin{cases} P_{\mathrm{load0}}^{t,\mathrm{SL,min}}\le P_{\mathrm{load0}}^{t,\mathrm{SL}}\le P_{\mathrm{load0}}^{t,\mathrm{SL,max}} \quad (\mu_{1,lb},\mu_{1,ub}) \\ \sum_{t=1}^{T}P_{\mathrm{load0}}^{t,\mathrm{SL}}=0 \quad (\lambda_1) \end{cases} \tag{4}$$

where $P_{\mathrm{load0}}^{t,\mathrm{SL}}$ is the time-shifted electricity load of RIES at time t; $P_{\mathrm{load0}}^{t,\mathrm{SL,max}}$ and $P_{\mathrm{load0}}^{t,\mathrm{SL,min}}$ are the maximum and minimum limits of the time-shifted electricity load of RIES at time t, respectively; and $\mu_{1,lb}$, $\mu_{1,ub}$, and λ_1 are the allocated Lagrange multipliers.

IL: it is a form of electricity consumption where users can interrupt a portion of their load during periods of inadequate power supply or high electricity prices to alleviate pressure on the power grid [22]. The characteristics of IL can be described as:

$$P_{\mathrm{load0}}^{t,\mathrm{IL,min}}\le P_{\mathrm{load0}}^{t,\mathrm{IL}}\le P_{\mathrm{load0}}^{t,\mathrm{IL,max}} \quad (\mu_{2,lb},\mu_{2,ub}) \tag{5}$$

where $P_{\mathrm{load0}}^{t,\mathrm{IL,max}}$ and $P_{\mathrm{load0}}^{t,\mathrm{IL,min}}$ are the maximum and minimum limits of interruptible electricity load for RIES at time t, respectively; and $\mu_{2,lb}$ and $\mu_{2,ub}$ are the allocated Lagrange multipliers.

The motivation for demand response for heating is the fact that users have a certain degree of tolerance or fuzziness in their perception of temperature. Furthermore, minor temperature adjustments within a specific range do not significantly impact the user's comfort experience [23]. This demand response behavior can be described as:

$$0\le H_{\mathrm{load0}}^{t,\mathrm{IL}}\le H_{\mathrm{load0}}^{t,\mathrm{IL,max}} \quad (\mu_{3,lb},\mu_{3,ub}) \tag{6}$$

where $H_{\mathrm{load0}}^{t,\mathrm{IL}}$ is the shiftable load at time t; $H_{\mathrm{load0}}^{t,\mathrm{IL,max}}$ is the maximum value of shiftable load at time t; and $\mu_{3,lb}$ and $\mu_{3,ub}$ are the allocated Lagrange multipliers.

RIES incorporates various types of electricity and heat loads. To comprehensively evaluate the impact of CDR implementation in the RIES on user experience, we introduce $f(E_{en}^{t})$ as the user utility function, representing the overall satisfaction derived from purchasing electricity and heat. Additionally, when users deviate from the most suitable baseline load E_{B}^{t} during each time period, their satisfaction is reduced to a certain extent, which is expressed as a function $f(E_{B}^{t})$.

$$\begin{cases} f(E_{en}^{t})=\sum_{en}\left(\alpha_{en}E_{en}^{t}-\dfrac{\beta_{en}}{2}(E_{en}^{t})^2\right) \\ f(E_{B}^{t})=\sum_{en\in E}\left(\dfrac{1}{2}\lambda_{en}\left|E_{en}^{t}-E_{B}^{t}\right|^2+\theta_{en}\left|E_{en}^{t}-E_{B}^{t}\right|\right) \end{cases} \tag{7}$$

where en represents the energy type; E is the set of energy types for user consumption; E_{en}^{t} is the actual load of energy en in the MG at time t; α_{en} and β_{en} are the preference coefficients for RIES users' energy consumption, which are related to the energy type; and λ_{en} and θ_{en} are the satisfaction loss parameters for energy en.

The specific representation of the actual response quantity E_{en}^{t} for the user can be expressed as:

$$\begin{cases} P_{\mathrm{load}}^{t}=P_{\mathrm{load0}}^{t}+P_{\mathrm{load0}}^{t,\mathrm{SL}}-P_{\mathrm{load0}}^{t,\mathrm{IL}} \quad (\lambda_2) \\ H_{\mathrm{load}}^{t}=H_{\mathrm{load0}}^{t}-H_{\mathrm{load0}}^{t,\mathrm{IL}} \quad (\lambda_3) \end{cases} \tag{8}$$

where P_{load0}^{t} and H_{load0}^{t} are the initial values of electricity and heat load, respectively; P_{load}^{t} and H_{load}^{t} are the magnitudes of electricity and heat loads after CDR, respectively; and λ_2 and λ_3 are the allocated Lagrange multipliers.

In conclusion, the benefit demands of RIES on the load side can be expressed by the maximization of a comprehensive utility function, which is denoted as:

$$\max US=\sum_{t=1}^{24}\left(f(E_{en}^{t})-f(E_{B}^{t})-\sum_{en\in E}E_{en}^{t}w_{en}\right) \tag{9}$$

where US is the comprehensive utility function of the user; and w_{en} is the electricity price set by the RIES.

III. TSDRGM Considering Wind Power Uncertainty

A. Objective Function

A TSDRGM is proposed for the daily and real-time operation of RIES operators. The first stage involves day-ahead scheduling, implemented as a Stackelberg game. The upper-level MG serves as the leader, while the lower-level users act as the followers. Using day-ahead forecasted wind power information, the upper-level MG determines energy prices and unit schedule plans, which are then communicated to the lower-level users. The lower-level users adjust their load demands through CDR, considering the upper-level information and providing feedback to the upper level. The day-ahead decision-making process is independent of wind power uncertainty. The second stage is the real-time rescheduling, which builds upon the decisions made in the day-ahead scheduling stage x. In this stage, flexible adjustments are made to the unit output to achieve optimal rescheduling costs $\boldsymbol{b}^{\mathrm{T}}\boldsymbol{y}$ under different scheduling decisions. To facilitate explanation, the entire process is simplified and represented in matrix form, described by (10)-(12).

$$\min_{\boldsymbol{x}}\left\{-\boldsymbol{a}^{\mathrm{T}}\boldsymbol{x}+\max_{\boldsymbol{d}\in\boldsymbol{D}}\left\{\sum_{k=1}^{K}P_k\min_{\boldsymbol{y}\in\boldsymbol{\Omega}(\boldsymbol{x},\boldsymbol{d})}\boldsymbol{b}^{\mathrm{T}}\boldsymbol{y}\right\}\right\} \tag{10}$$

$$\boldsymbol{C}\boldsymbol{x}\le\boldsymbol{g} \tag{11}$$

$$\boldsymbol{\Omega}(\boldsymbol{x},\boldsymbol{d})=\{\boldsymbol{y}:\boldsymbol{E}\boldsymbol{y}\le\boldsymbol{e},\boldsymbol{A}\boldsymbol{y}+\boldsymbol{B}\boldsymbol{d}=\boldsymbol{c},\boldsymbol{E}\boldsymbol{x}+\boldsymbol{F}\boldsymbol{y}\le\boldsymbol{h}\} \tag{12}$$

where $\boldsymbol{x}$ is the vector of decision variables in the day-ahead stage; $\boldsymbol{y}$ is the vector of decision variables in the real-time stage; $\boldsymbol{a}^{\mathrm{T}}\boldsymbol{x}$ is the revenue from energy sale of RIES operator in the day-ahead stage; $\boldsymbol{b}^{\mathrm{T}}\boldsymbol{y}$ is the system operating cost of RIES after adjustments in the real-time stage, which is influenced by uncertain parameter $\boldsymbol{d}$; K is the total number of clustering scenarios; P_k is the probability of an individual clustering scenario; $\boldsymbol{A}$, $\boldsymbol{B}$, $\boldsymbol{C}$, $\boldsymbol{E}$, and $\boldsymbol{F}$ are the matrices corresponding to relevant parameters; $\boldsymbol{a}$ and $\boldsymbol{b}$ are the column vectors of parameters in the objective function; and $\boldsymbol{c}$, $\boldsymbol{e}$, $\boldsymbol{g}$, and $\boldsymbol{h}$ are the column vectors of parameters under constraint conditions.

$$\begin{cases}\boldsymbol{x}=[P_{\mathrm{GT}}^{t},H_{\mathrm{GT}}^{t},H_{\mathrm{GB}}^{t},P_{\mathrm{Grid}}^{t,\mathrm{buy}},P_{\mathrm{Grid}}^{t,\mathrm{sell}},E_{\mathrm{CES}},E_{\mathrm{CES}}^{\max},P_{\mathrm{CES}}^{\mathrm{ch}},u_{\mathrm{CES}}^{t,\mathrm{ch}},\\ \quad P_{\mathrm{CES}}^{\mathrm{dis}},u_{\mathrm{CES}}^{t,\mathrm{dis}},E_{\mathrm{CTS}},E_{\mathrm{CTS}}^{\max},P_{\mathrm{CTS}}^{\mathrm{ch}},u_{\mathrm{CTS}}^{t,\mathrm{ch}},P_{\mathrm{CTS}}^{\mathrm{dis}},u_{\mathrm{CTS}}^{t,\mathrm{dis}},U_{\mathrm{Grid}}^{t},\\ \quad P_{\mathrm{load}}^{t},H_{\mathrm{load}}^{t},P_{\mathrm{load0}}^{t,\mathrm{SL}},P_{\mathrm{load0}}^{t,\mathrm{IL}},H_{\mathrm{load0}}^{t,\mathrm{IL}}]^{\mathrm{T}}\\ \boldsymbol{y}=[P_{\mathrm{WT}}^{t},\tilde{P}_{\mathrm{GT}}^{t,\mathrm{up}},\tilde{P}_{\mathrm{GT}}^{t,\mathrm{down}},\tilde{H}_{\mathrm{GB}}^{t,\mathrm{up}},\tilde{H}_{\mathrm{GB}}^{t,\mathrm{down}},\tilde{P}_{\mathrm{Grid}}^{t,\mathrm{buy}},\tilde{P}_{\mathrm{Grid}}^{t,\mathrm{sell}},E_{\mathrm{CES}}^{t},\\ \quad \tilde{P}_{\mathrm{CES}}^{\mathrm{ch}},\tilde{P}_{\mathrm{CES}}^{\mathrm{dis}},E_{\mathrm{CTS}}^{t},\tilde{P}_{\mathrm{CTS}}^{\mathrm{ch}},\tilde{P}_{\mathrm{CTS}}^{\mathrm{dis}}]^{\mathrm{T}}\end{cases} \tag{13}$$

where E_{CES}^{t} and E_{CTS}^{t} are the capacities of CES and CTS at time t, respectively; E_{CES} and E_{CTS} are the rented energy storage capacities of CES and CTS, respectively; $E_{\mathrm{CES}}^{\max}$ and $E_{\mathrm{CTS}}^{\max}$ are the maximum rented energy capacities of CES and CTS, respectively; $P_{\mathrm{CES}}^{\mathrm{ch}}$ and $P_{\mathrm{CES}}^{\mathrm{dis}}$ are the charging and discharging power limits for rented CES, respectively; $P_{\mathrm{CTS}}^{\mathrm{ch}}$ and $P_{\mathrm{CTS}}^{\mathrm{dis}}$ are the charging and discharging power limits for rented CTS, respectively; $u_{\mathrm{CES}}^{t,\mathrm{ch}}$ and $u_{\mathrm{CES}}^{t,\mathrm{dis}}$ are the binary variables indicating the charging or discharging state of CES, respectively; $u_{\mathrm{CTS}}^{t,\mathrm{ch}}$ and $u_{\mathrm{CTS}}^{t,\mathrm{dis}}$ are the binary variables indicating the charging or discharging state of CTS, respectively; $\tilde{P}_{\mathrm{Grid}}^{t,\mathrm{buy}}$ and $\tilde{P}_{\mathrm{Grid}}^{t,\mathrm{sell}}$ are the power adjustments for purchasing and selling electricity from/to the main grid at time t, respectively; $\tilde{P}_{\mathrm{GT}}^{t,\mathrm{up}}$ and $\tilde{P}_{\mathrm{GT}}^{t,\mathrm{down}}$ are the upward and downward adjustments of electric power for GT at time t, respectively; $\tilde{H}_{\mathrm{GB}}^{t,\mathrm{up}}$ and $\tilde{H}_{\mathrm{GB}}^{t,\mathrm{down}}$ are the upward and downward adjustments of heating power for GB at time t, respectively; $\tilde{P}_{\mathrm{CES}}^{\mathrm{ch}}$ and $\tilde{P}_{\mathrm{CES}}^{\mathrm{dis}}$ are the power adjustments for charging and discharging of CES at time t, respectively; and $\tilde{P}_{\mathrm{CTS}}^{\mathrm{ch}}$ and $\tilde{P}_{\mathrm{CTS}}^{\mathrm{dis}}$ are the power adjustments for charging and discharging of CHS at time t, respectively.

Moreover, given the challenge of acquiring the probability density function of actual wind power scenarios, this study utilizes historical wind power data. It implements the K-means clustering algorithm to identify representative discrete scenarios. The information of the initial scenario probability density P_{k0} is obtained, aiming to maximize the expected operating cost for the worst-case distribution among these typical scenarios. The values of $\{P_k\}$ is chosen regarding the benchmark fluctuations of P_{k0}. According to [24], $\{P_k\}$ is subject to the following confidence constraints:

$$\begin{cases}\Pr\left\{\sum_{k=1}^{K}\left|P_k-P_{k0}\right|\le\theta_1\right\}\ge 1-2K\mathrm{e}^{-2V\theta_1/K}\\ \Pr\left\{\max_{1\le k\le K}\left|P_k-P_{k0}\right|\le\theta_\infty\right\}\ge 1-2K\mathrm{e}^{-2V\theta_\infty}\end{cases} \tag{14}$$

where θ_1 and θ_∞ are the allowable deviation values for the 1-norm and ∞-norm probabilities, respectively; and V is the historical data sample. Additionally, we set the right-hand side of (14) to a given confidence level, denoted as δ_1 and δ_∞.

1) Day-ahead Objective Function $C_{\mathrm{Day-ahead}}^{t}$

In the day-ahead stage, it is necessary to ensure the reliable supply of wind power consumption and load safety. The objective function of the day-ahead scheduling includes the US objective function, gas purchasing cost of RIES C_{g}, operating cost of WT C_{WT}, operating cost of CESS C_{CESS}, carbon trading cost C_{CC}, and cost of interaction power with the main grid C_{Grid}.

$$\begin{cases}C_{\mathrm{Day-ahead}}^{t}=-US+C_{\mathrm{g}}+C_{\mathrm{WT}}+C_{\mathrm{CESS}}+C_{\mathrm{CC}}+C_{\mathrm{Grid}}\\ C_{\mathrm{g}}=\sum_{t=1}^{24}c_{\mathrm{g}}^{t,\mathrm{buy}}G^{t,\mathrm{buy}}\\ C_{\mathrm{WT}}=\sum_{t=1}^{24}c_{\mathrm{WT}}P_{\mathrm{WT}}^{t}\\ C_{\mathrm{Grid}}=\sum_{t=1}^{24}(P_{\mathrm{Grid}}^{t,\mathrm{buy}}c_{\mathrm{Grid}}^{t,\mathrm{buy}}-P_{\mathrm{Grid}}^{t,\mathrm{sell}}c_{\mathrm{Grid}}^{t,\mathrm{sell}})\\ C_{\mathrm{CC}}=C_{co_2}\sum_{t=1}^{24}[\gamma_{\mathrm{GT}}P_{\mathrm{GT}}^{t}+\gamma_{\mathrm{GB}}H_{\mathrm{GB}}^{t}+\gamma_{\mathrm{Grid}}(P_{\mathrm{Grid}}^{t,\mathrm{buy}}-P_{\mathrm{Grid}}^{t,\mathrm{sell}})]\\ C_{\mathrm{CESS}}=\sum_{i\in\Omega_{\mathrm{CESS}}}\sum_{t=1}^{24}[(\lambda_{\mathrm{E}}E_{i}^{t}+\lambda_{\mathrm{P}}P_{i}^{t,\mathrm{ch}}+\lambda_{\mathrm{P}}P_{i}^{t,\mathrm{dis}})/365]+\\ \qquad\sum_{i\in\Omega_{\mathrm{CESS}}}\sum_{t=1}^{24}\lambda_{\mathrm{on}}(P_{i}^{t,\mathrm{ch}}+P_{i}^{t,\mathrm{dis}})\end{cases} \tag{15}$$

where $c_{\mathrm{g}}^{t,\mathrm{buy}}$ is the gas purchasing price at time t; $G^{t,\mathrm{buy}}$ is the

quantity of gas purchased at time t; c_{WT} is the actual power output of WT at time t; $P_{\mathrm{Grid}}^{t,\mathrm{buy}}$ and $P_{\mathrm{Grid}}^{t,\mathrm{sell}}$ are the power interactions between the MG and the main grid at time t; $c_{\mathrm{Grid}}^{t,\mathrm{buy}}$ and $c_{\mathrm{Grid}}^{t,\mathrm{sell}}$ are the prices of power interaction between the MG and the main grid at time t; C_{co_2} is the carbon tax price; γ_{GT} and γ_{GB} are the carbon emission coefficients corresponding to the unit power output of GT and GB, respectively; γ_{Grid} is the carbon emission coefficient for electricity generation from the grid; P_{GT}^{t} is the electric power output of GT at time t; H_{GB}^{t} is the heating power output of GB at time t; Ω_{CESS} is the collection of CESSs; E_i^t is the capacity of CSEE i at time t; $P_i^{t,\mathrm{ch}}$ and $P_i^{t,\mathrm{dis}}$ are the charging and discharging power of CSEE, respectively; λ_{E} and λ_{P} are the leasing costs per unit capacity and per unit power for CESS, respectively; and λ_{on} is a coefficient representing operating and maintenance costs for charging/discharging operations of CESS.

2) Real-time Objective Function $C_{\mathrm{Real-time}}^{t}$

Real-time adjustments are implemented in the day-ahead schedule to manage wind power forecasting errors effectively. Methods such as rescheduling and wind curtailment are employed to address these errors. It is important to highlight that in RIES, load demand response is guided in the preceding stage by establishing peak/off-peak TOU energy prices, which helps form rational load plans. However, CDR from the load side necessitates pre-signed contracts. As a result, the load side determines its response plan in the prior stage, and this response remains unchanged in the real-time stage. The objective function of the rescheduling includes the main grid interaction rescheduling cost D_{Grid}, wind curtailment penalty cost D_{cut}, and generator power adjustment cost D_{UC}.

$$\begin{cases} C_{\mathrm{Real-time}}^{t} = D_{\mathrm{Grid}} + D_{\mathrm{cut}} + D_{\mathrm{UC}} \\ D_{\mathrm{Grid}} = \sum_{t=1}^{24} (d_{\mathrm{Grid}}^{t,\mathrm{buy}} \tilde{P}_{\mathrm{Grid}}^{t,\mathrm{buy}} + c_{\mathrm{g}}^{t,\mathrm{buy}} \tilde{G}^{t,\mathrm{buy}} - d_{\mathrm{Grid}}^{t,\mathrm{sell}} \tilde{P}_{\mathrm{Grid}}^{t,\mathrm{sell}}) \\ D_{\mathrm{cut}} = \sum_{t=1}^{24} c_{qf} \tilde{P}_{\mathrm{WT}}^{t,\mathrm{cut}} \\ D_{\mathrm{UC}} = \sum_{t=1}^{24} (d_{\mathrm{GT}}^{t,\mathrm{up}} \tilde{P}_{\mathrm{GT}}^{t,\mathrm{up}} + d_{\mathrm{GT}}^{t,\mathrm{down}} \tilde{P}_{\mathrm{GT}}^{t,\mathrm{down}}) + \\ \qquad \sum_{t=1}^{24} (d_{\mathrm{GB}}^{t,\mathrm{up}} \tilde{H}_{\mathrm{GB}}^{t,\mathrm{up}} + d_{\mathrm{GB}}^{t,\mathrm{down}} \tilde{H}_{\mathrm{GB}}^{t,\mathrm{down}}) \end{cases} \tag{16}$$

where $d_{\mathrm{Grid}}^{t,\mathrm{buy}}$ and $d_{\mathrm{Grid}}^{t,\mathrm{sell}}$ are the real-time prices at which the MG purchases or sells electricity from/to the main grid, respectively; c_{qf} is the wind curtailment penalty coefficient; $\tilde{P}_{\mathrm{WT}}^{t,\mathrm{cut}}$ is the wind power adjustment in the MG at time t; $d_{\mathrm{GT}}^{t,\mathrm{up}}$ and $d_{\mathrm{GT}}^{t,\mathrm{down}}$ are the upward and downward penalty coefficients for the power adjustment of GT in the MG, respectively; and $d_{\mathrm{GB}}^{t,\mathrm{up}}$ and $d_{\mathrm{GB}}^{t,\mathrm{down}}$ are the upward and downward penalty coefficients for the power adjustment of GB in the MG, respectively.

B. Day-ahead Scheduling Constraints

1) Energy Price Constraints

To ensure the coordination of user interests, the average value of TOU energy prices set by the operator should not surpass the initial selling price of energy. This constraint can be expressed as (taking electricity price as an example):

$$\begin{cases} w_{\mathrm{e}}^{\min} \le w_{\mathrm{e}}^{t} \le w_{\mathrm{e}}^{\max} \\ \sum_{t=1}^{T} w_{\mathrm{e}}^{t} \le T w_{\mathrm{e}}^{\mathrm{in}} \end{cases} \tag{17}$$

where T is the scheduling period; w_{e}^{t} is the energy price; $w_{\mathrm{e}}^{\max}$ and $w_{\mathrm{e}}^{\min}$ are the maximum and minimum values of the set electricity price, respectively; and $w_{\mathrm{e}}^{\mathrm{in}}$ is the initially set electricity price. The process of setting heat prices follows a similar approach and will not be further detailed in this context.

2) Operational Constraints of Main Grid

$$\begin{cases} 0 \le P_{\mathrm{Grid}}^{t,\mathrm{buy}} \le U_{\mathrm{Grid}}^{t} P_{\mathrm{Grid}}^{t,\mathrm{buy,max}} \\ 0 \le P_{\mathrm{Grid}}^{t,\mathrm{sell}} \le (1 - U_{\mathrm{Grid}}^{t}) P_{\mathrm{Grid}}^{t,\mathrm{sell,max}} \end{cases} \tag{18}$$

where $P_{\mathrm{Grid}}^{t,\mathrm{buy,max}}$ and $P_{\mathrm{Grid}}^{t,\mathrm{sell,max}}$ are the maximum values of electricity purchasing from and selling to the main grid by the MG, respectively; and U_{Grid}^{t} is the status that represents the electricity purchasing from or selling to the main grid by the MG at time t.

3) Operational Constraints of Natural Gas Network

$$0 \le G^{t,\mathrm{buy}} \le G^{t,\mathrm{buy,max}} \tag{19}$$

where $G^{t,\mathrm{buy,max}}$ is the maximum value of the gas purchased for the MG.

4) Wind Power Output Constraints

$$0 \le P_{\mathrm{WT}}^{t} \le P_{\mathrm{WT}}^{t,\mathrm{pre}} \tag{20}$$

where $P_{\mathrm{WT}}^{t,\mathrm{pre}}$ is the predicted value of WT output power at time t.

5) Power Balance Constraints

$$\begin{cases} P_{\mathrm{GT}}^{t} + P_{\mathrm{WT}}^{t} + P_{\mathrm{CES}}^{t,\mathrm{dis}} + P_{\mathrm{Grid}}^{t,\mathrm{buy}} = P_{\mathrm{load}}^{t} + P_{\mathrm{CES}}^{t,\mathrm{ch}} + P_{\mathrm{Grid}}^{t,\mathrm{sell}} \\ H_{\mathrm{GT}}^{t} + H_{\mathrm{GB}}^{t} + P_{\mathrm{CTS}}^{t,\mathrm{dis}} = H_{\mathrm{load}}^{t} + P_{\mathrm{CTS}}^{t,\mathrm{ch}} \end{cases} \tag{21}$$

where $P_{\mathrm{CES}}^{t,\mathrm{ch}}$ and $P_{\mathrm{CES}}^{t,\mathrm{dis}}$ are the charging and discharging power of CES at time t, respectively; and $P_{\mathrm{CTS}}^{t,\mathrm{ch}}$ and $P_{\mathrm{CTS}}^{t,\mathrm{dis}}$ are the charging and discharging power of CTS at time t, respectively.

In addition to the above-mentioned constraints (17)-(21), the day-ahead scheduling stage also includes additional constraints related to the thermal-coupled supply system, CESS, and CDR constraints. These constraints are described in (1)-(6), which will not be reiterated here.

C. Real-time Rescheduling Constraints

Based on the day-ahead scheduling, RIES undergoes real-time rescheduling to make adjustments. It is important to ensure that the adjusted output of each device satisfies its respective operational constraints and system power balance constraints. Specifically, the real-time rescheduling constraints are modified by altering the day-ahead scheduling decision variables in (1)-(3), (18), and (21). As an example, the constraint for GB in (2) can be modified as:

$$\begin{cases} H_{\mathrm{GB}}^{t,\min} \le H_{\mathrm{GB}}^{t} + \tilde{H}_{\mathrm{GB}}^{t,\mathrm{up}} - \tilde{H}_{\mathrm{GB}}^{t,\mathrm{down}} \le H_{\mathrm{GB}}^{t,\max} \\ \tilde{H}_{\mathrm{GB}}^{t,\mathrm{up,min}} \le \tilde{H}_{\mathrm{GB}}^{t,\mathrm{up}} \le \tilde{H}_{\mathrm{GB}}^{t,\mathrm{up,max}} \\ \tilde{H}_{\mathrm{GB}}^{t,\mathrm{down,min}} \le \tilde{H}_{\mathrm{GB}}^{t,\mathrm{down}} \le \tilde{H}_{\mathrm{GB}}^{t,\mathrm{down,max}} \end{cases} \tag{22}$$

where $\tilde{H}_{\mathrm{GB}}^{t,\mathrm{up,min}}$ and $\tilde{H}_{\mathrm{GB}}^{t,\mathrm{up,max}}$ are the minimum and maximum up adjustable power of GB at time t, respectively; and $\tilde{H}_{\mathrm{GB}}^{t,\mathrm{down,min}}$ and $\tilde{H}_{\mathrm{GB}}^{t,\mathrm{down,max}}$ are the minimum and maximum downward adjustable power of GB at time t, respectively.

IV. Uniqueness of Game Equilibrium Solution and Model Solving

A. Proof of Uniqueness of Game Equilibrium Solution

In the Stackelberg game, the RIES operator serves as the leader, while the users on the RIES side act as followers. When the game between the RIES operator and its users reaches a Nash equilibrium (NE), which maximizes their respective interests, no party can unilaterally change the NE to obtain greater benefits. The Stackelberg game model exhibits a unique NE when the following conditions are met: the objective functions of all participants are non-empty and continuous functions with respect to their respective strategy sets. The objective function of each follower is a continuous convex or concave function with respect to their own strategy set.

Proof: in the game, the leader is the RIES operator, and its objective function is given by (15), which is non-empty and continuous. The followers are the users on the RIES side, and their objective function is the time-dependent power consumption, represented by (17), which has a non-empty and continuous decision set. The utility function of the game-following user is differentiated to obtain the second-order partial derivatives concerning its decision variables in the game. The value of this derivative is $-(\beta_{en}+\lambda_{en})$, where β_{en} and λ_{en} are the positive real numbers, and $-(\beta_{en}+\lambda_{en})<0$. Therefore, the *US* is a continuous convex function concerning its strategy set. Based on these observations, it can be concluded that the described Stackelberg game model has a unique NE.

B. Equivalence Between KKT Conditions and Linearization of Bilinear Terms

The TSDRGM constructed in this study encompasses a two-level Stackelberg game model in the day-ahead scheduling stage. The coupling between the upper-level and lower-level models poses difficulties in direct solution. The Lagrangian function of the lower-level model is formulated to address this challenge, and the KKT complementary relaxation conditions [25] are applied based on the lower-level model. This transformation enables the lower-level model to be represented as a constraint for the upper-level model. Subsequently, the resulting transformed model, now a single-level nonlinear model, can be linearized using the big-*M* method [26]. This linearization process facilitates the formulation of a mixed-integer linear programming problem. Additionally, since the revenue $\sum_{t=1}^{24}\sum_{i\in\Omega_{energy}} w_i^t P_i^{t,\text{sell}}$ from energy sales by the RIES operator involves bilinear terms that cannot be directly solved, linear equivalence can be obtained using derived KKT equations. w_i^t is the price of energy; $P_i^{t,\text{sell}}$ is the power sold by energy; and Ω_{energy} is the energy type collection. The transformation process mentioned above is detailed in the Supplementary Material A.

C. Reconstruction of Distributionally Robust Optimization Mode

Upon applying the KKT equivalent transformation, (10) is transformed into a three-level optimization problem in the form of min-max-min. The optimization variables in the day-ahead and real-time stages are interconnected, making direct solutions unattainable. To overcome this challenge, the C&CG algorithm decomposes the model into a master problem (MP) and sub-problems (SPs). The solution process using C&CG algorithm is shown in Fig. 2, where $\boldsymbol{P}_0$ is the initial probability distribution; p_k^0 is the specific probability value; $\boldsymbol{x}^*$ denotes the results of the day-ahead scheduling variable solutions; $(\boldsymbol{d}^l)^*$ denotes the worst-case uncertainty parameters for the l^{th} iteration; γ is the auxiliary variable; and ε is the convergence coefficient.

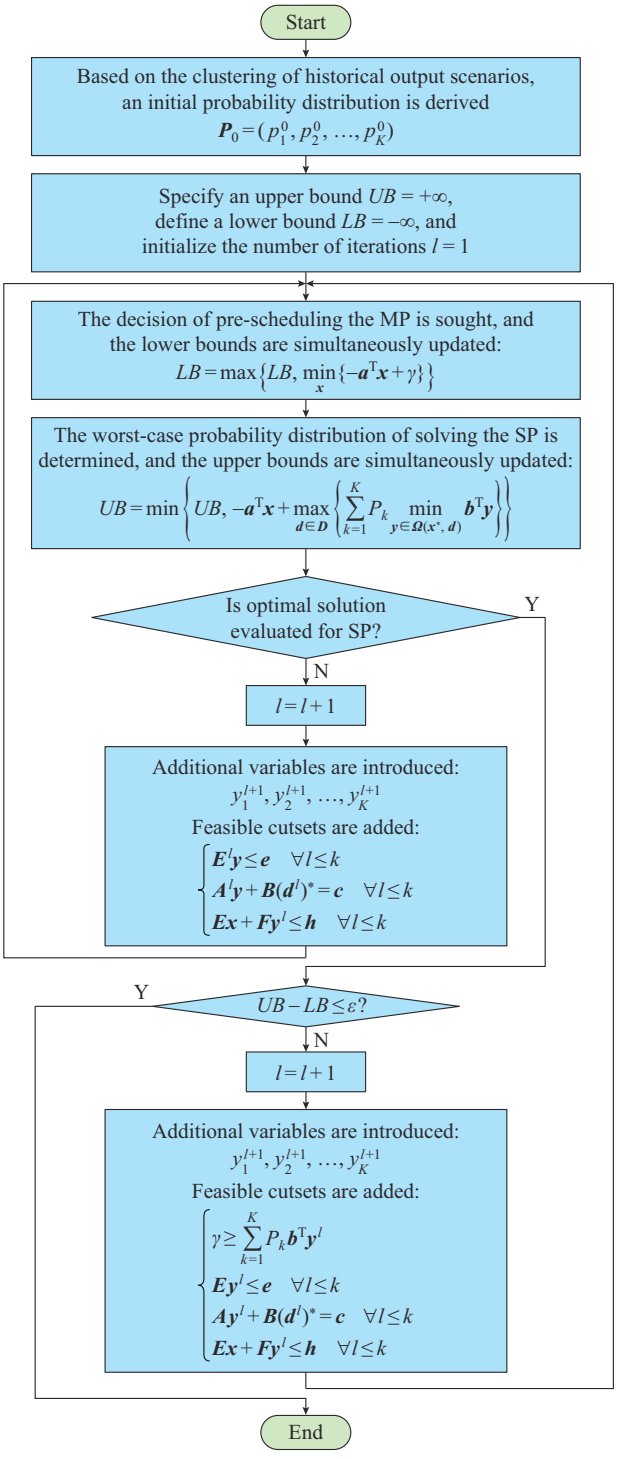

Fig. 2. Diagram of solution process using C&CG algorithm.

This decomposition efficiently converts the three-level optimization model into a more manageable structure. For detailed solution procedures, please refer to [27].

V. Case Analysis

To evaluate the effectiveness of the proposed strategy for RIES, an actual RIES in north China was chosen for simulation analysis. The optimization problem was solved using MATLAB R2018b software with the YALMIP plugin and the Cplex solver. The computer configuration comprised an Intel Core i7 processor with a clock frequency of 1.8 GHz and 16 GB of memory. For the case study, typical daily data from a specific region in north China were chosen as the background. The initial load curve and wind power forecasting curve are presented in Fig. 3, and the main parameters are listed in Table I, where $\lambda_{\mathrm{E,CES}}$ and $\lambda_{\mathrm{E,CTS}}$ are the price coefficients of CSE and CTS capacities, respectively; $\lambda_{\mathrm{P,CES}}$ and $\lambda_{\mathrm{P,CTS}}$ are the price coefficients of CES and CTS power, respectively; $\lambda_{\mathrm{on,CES}}$ and $\lambda_{\mathrm{on,CTS}}$ are the price coefficients of charging and discharging during CES and CTS operation, respectively; α_e, β_e, α_h, and β_h are the utility coefficients of energy; $\tilde{P}^{\mathrm{ch,max}}_{\mathrm{CESS}}$ and $\tilde{P}^{\mathrm{dis,max}}_{\mathrm{CESS}}$ are the maximum values of charging and discharging adjustment power of CESS, respectively. The interactive electricity price between the RIES and the main grid is listed in Fig. 4. These data are used to validate and demonstrate the performance of the proposed strategy in optimizing RIES operations.

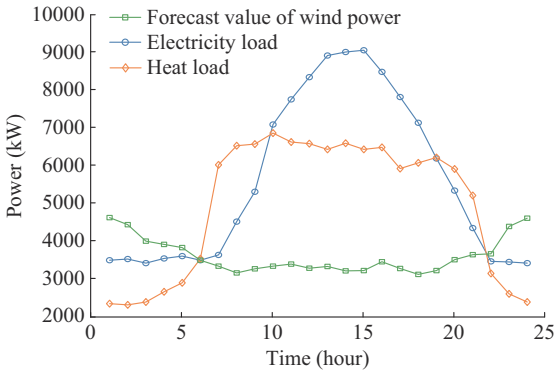

Fig. 3. Initial load curve and wind power forecast curve.

TABLE I
Main Parameters

Parameter	Value	Parameter	Value
$P^{t,\mathrm{buy,max}}_{\mathrm{Grid}}$	2000 kW	$P^{\mathrm{ch,max}}_{\mathrm{CESS}}$	150 kW
$P^{t,\mathrm{sell,max}}_{\mathrm{Grid}}$	2000 kW	$P^{\mathrm{dis,max}}_{\mathrm{CESS}}$	150 kW
$\tilde{P}^{t,\mathrm{buy}}_{\mathrm{Grid}}$	500 kW	α_e	2
$\tilde{P}^{t,\mathrm{sell}}_{\mathrm{Grid}}$	500 kW	β_e	0.008
$\lambda_{\mathrm{E,CES}}$	110 CNY/kW	α_h	3
$\lambda_{\mathrm{P,CES}}$	37 CNY/kW	β_h	0.015
$\lambda_{\mathrm{on,CES}}$	0.01 CNY/kW	$H^{t,\mathrm{max}}_{\mathrm{GB}}$	1000 kW
$\lambda_{\mathrm{E,CTS}}$	30 CNY/kW	$P^{t,\mathrm{max}}_{\mathrm{GT}}$	5000 kW
$\lambda_{\mathrm{P,CTS}}$	10 CNY/kW	$\tilde{H}^{t,\mathrm{up}}_{\mathrm{GB}}$	200 kW
$\lambda_{\mathrm{on,CTS}}$	0.005 CNY/kW	$\tilde{H}^{t,\mathrm{down}}_{\mathrm{GB}}$	200 kW
$\tilde{P}^{\mathrm{ch,max}}_{\mathrm{CESS}}$	150 kW	$\tilde{P}^{t,\mathrm{up}}_{\mathrm{GT}}$	500 kW
$\tilde{P}^{\mathrm{dis,max}}_{\mathrm{CESS}}$	150 kW	$\tilde{P}^{t,\mathrm{down}}_{\mathrm{GT}}$	500 kW

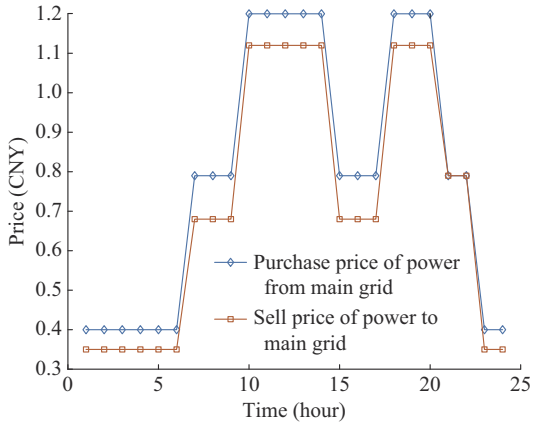

Fig. 4. Interactive electricity prices between RIES and main grid.

A. Iteration Results

In order to validate the feasibility of the proposed strategy, this subsection conducts an analysis using ten sets of typical scenarios from various historical data. The relationship among the total operating cost of the RIES, the computational time of the program, and the number of scenarios is examined. The results of this analysis are visually presented in Fig. 5.

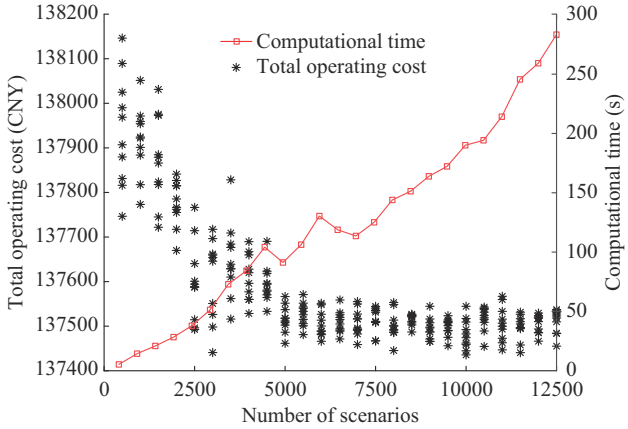

Fig. 5. Relationship among total operating cost, computational time, and number of scenarios.

It can be observed from Fig. 4 that when the amount of historical data is small, the distribution of the total operating cost exhibits a higher variance and divergence. However, as the number of scenarios increases, the variance decreases, and the distribution stabilizes. This analysis suggests that the system is more susceptible to risk disturbances with fewer data samples, leading to more varied scheduling decisions in robust optimization scheduling under uncertainty. As more historical data become available, the exposure of the system to risk disturbances decreases, and the solution space of the robust game optimization problem converges, resulting in a more concentrated cost distribution.

Moreover, although the computational time of the model fluctuates and increases with an increasing number of scenarios, it remains within acceptable limits for day-ahead scheduling, considering the computing hardware conditions mentioned in this study.

Additionally, as computing hardware conditions improve, computational speed is likely to increase significantly, meeting the requirement for computational efficiency. Considering the relationship among the total operating cost, computational time, and number of scenarios, this study selects 5000 historical data samples and ten discrete scenarios to solve the TSDRGM. The determined energy selling prices of RIES, as shown in Fig. 6, are reasonable and fall within an acceptable range for users when compared with external energy prices for MGs.

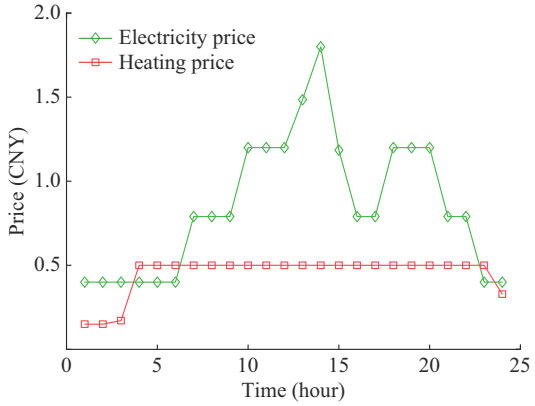

Fig. 6. Energy selling prices of RIES.

B. Comparative Analysis

1) Comparative Analysis of Parameters

Equation (14) shows that different confidence levels correspond to different bias limits when given a set of V samples.

This analysis aims to assess how the comprehensive norm constraints enforced by the 1-norm and ∞-norm sets in the TSDRGM affect the total operating cost of RIES. In this part, 5000 historical data samples are selected to examine variations in scheduling costs within the TSDRGM at varying confidence levels. Table II illustrates the impact of confidence levels on the total operating cost of RIES.

TABLE II
IMPACT OF CONFIDENCE LEVELS ON TOTAL OPERATING COST OF RIES

δ_∞	Total operating cost (CNY)			
	$\delta_1=0.3$	$\delta_1=0.5$	$\delta_1=0.7$	$\delta_1=0.99$
0.50	136600.92	136909.02	137345.91	137388.62
0.70	137025.63	137114.97	137480.23	137500.09
0.85	137203.20	137316.51	137527.74	137592.13
0.99	137321.79	137514.22	137656.22	137682.27

Based on Table II, it is evident that when employing comprehensive norm constraints, the total operating cost of RIES gradually increases as the combined value of the confidence levels δ_1 and δ_∞ increases. Notable, δ_∞ has a more pronounced impact on the outcomes. This phenomenon can be intuitively explained: a higher confidence level indicates a greater likelihood of encountering a worst-case scenario in the output power of renewable energy sources, indicating an increase in the uncertainty covered by the optimization problem. In such cases, the RIES adopts a more conservative strategy, requiring the allocation of more power output from controllable units to cope with the worst-case scenario of wind power output. As a result, the electricity sales profit of RIES is reduced, the integration of wind and solar energy is declined, and the total operating costs of the system are increased.

The above analysis indicates that by adjusting the combined value of confidence levels δ_1 and δ_∞, the robustness and economic efficiency of the adaptive balancing scheduling scheme can be effectively balanced. In the following examples, unless otherwise specified, δ_1 is set to be 0.50, and δ_∞ is set to be 0.99.

2) Comparison of Uncertainty Optimization Strategies

To assess the superiority of the proposed strategy, this study conducted a comparison with deterministic optimization (strategy 1), two-stage stochastic optimization (strategy 2), and two-stage robust optimization (strategy 3).

The impact of different optimization scheduling strategies on the costs of RIES is shown in Table III. It is evident that strategy 1 results in the lowest total operating cost. This is because strategy 1 assumes accurate forecast scenarios of wind power output, leading to a heavy reliance on purchasing electricity from the main grid to compensate for the power deficit due to forecast errors. However, this strategy underestimates the uncertainty risk associated with wind power and poses significant risks to the safe and stable operation of the system.

TABLE III
IMPACT OF DIFFERENT OPTIMIZATION SCHEDULING STRATEGIES ON COSTS OF RIES

Strategy	Total operating cost (CNY)	Day-ahead scheduling cost (CNY)	Real-time scheduling cost (CNY)	Computational efficiency (s)
1	92915.01	92915.01		63.50
2	105780.17	102888.67	2891.50	66.50
3	240649.88	210289.13	30360.75	84.20
Proposed	137514.22	128839.69	8674.50	90.05

In uncertainty optimization, strategy 2 yields the lowest day-ahead and real-time scheduling costs. This is because strategy 2 models the day-ahead scheduling scenarios of wind power based on accurate information about the probability density function of uncertain input parameters, thus enhancing economic efficiency and overall performance. Indeed, relying solely on precise probability distributions in strategy 2 may lead to overly optimistic expectations of real-time risks, making the system less robust to extreme wind power output scenarios and potentially leading to failure.

Strategy 3 has the highest day-ahead and real-time scheduling costs. This is because it relies on predetermined ranges for variable fluctuations during day-ahead scheduling, aiming to ensure results applicable in "worst-case" scenarios with a low probability of occurrence. In real-time decision-making, it prioritizes robustness by primarily increasing energy reserves to mitigate risks in real-time scheduling, often at the expense of economic efficiency. However, strategy 3 balances stochastic and robust optimization, yielding a total op-

erating cost that falls between the two. This strategy utilizes the worst-case probability distribution of forecast errors for day-ahead scheduling while incorporating probabilistic information from historical data. It achieves a trade-off between economic efficiency and robustness, making it a promising solution for RIES optimization.

3) Comparison and Analysis of Game-theoretic Methods

In this part, the effectiveness of the proposed model in the strategies for mitigating wind power uncertainty risk is validated by comparing it with the deterministic game model (model 1). The initial scenario probabilities are identical for both models. An error range of 0-40% is considered to explore the impact of wind power forecast errors, with a 10% increment for each scenario. Simulations are conducted for both models, and the results are presented in Table IV, which shows the robustness and efficiency of the proposed model in handling uncertainties and optimizing the RIES operation.

TABLE IV
COMPARISON OF RESULTS UNDER DIFFERENT MODELS

Model	ρ (%)	Total operating cost (CNY)	Wind power curtailment rate (%)	System carbon emission cost (CNY)	Energy sale revenue (CNY)	Computational efficiency (s)
1	0	137416.17	2.62	–4698.89	38289.42	62.60
	10	137488.19	4.89	–4476.27	38252.39	63.50
	20	137782.41	5.32	–4394.71	38231.27	64.30
	30	137910.98	5.84	–4236.45	38198.76	66.20
	40	138245.13	6.27	–4175.33	38183.81	69.50
Proposed	0	137416.17	2.62	–4698.89	38289.42	83.52
	10	137514.22	4.91	–4482.84	38123.91	90.05
	20	137634.16	4.96	–4479.69	38021.76	98.23
	30	137758.08	5.25	–4475.24	37848.59	105.20
	40	137865.12	5.78	–4473.52	37684.35	120.20

When the wind power forecast error is 0, both model 1 and the proposed model produce the same results. This is because the wind power output consistently aligns with the initial scenario probability distribution, leaving no room for deviations in either model. As the wind power forecast error gradually increases, the overall energy sales revenue of model 1 surpasses that of the proposed model. This discrepancy arises from the ability of model 1 to accurately predict wind power generation during day-ahead scheduling, allowing the operator to effectively optimize energy sale revenue while ensuring that the load demand is adequately met. The proposed model, on the other hand, incorporates a conservative approach to handle uncertainties, which may lead to slightly lower energy sales revenue as a precautionary measure against potential deviations in wind power output. During the real-time scheduling stage, the proposed model adjusts equipment power and energy sales revenue values based on real-time wind power scenarios, effectively compensating for wind power uncertainty. To mitigate risks, the operator adopts a more cautious energy sales strategy, often resorting to purchasing electricity from the main grid to ensure an adequate energy supply.

Consequently, the proposed model reduces the energy sales revenue compared with a more aggressive strategy. Upon analyzing Table IV, it becomes apparent that when the forecast error remains below 10%, model 1 exhibits lower operating costs than the proposed model. This is mainly due to the influence of variations in initial forecast errors on energy sales costs, with model 1 achieving higher energy sales revenue by adopting a more optimistic stance. However, as the forecast error surpasses 10%, the adaptability of demand response plans of model 1, formulated during day-ahead scheduling, significantly diminishes compared with the proposed model. Consequently, the original scheduling plan fails to meet the actual load demands. To compensate for these discrepancies, RIES operators rely heavily on controllable units to manage the fluctuations in wind power.

Consequently, during situations involving substantial changes in wind power forecast errors, model 1 exhibits higher curtailment rates and carbon emission costs compared with the proposed model. In summary, the proposed model fully accounts for forecast errors in wind power generation during decision-making, offering enhanced uncertainty-handling capabilities. It effectively optimizes the power interaction between the RIES and the main grid, especially in the case of significant forecast errors. This optimization reduces curtailment rates and carbon emissions, thereby improving the operational efficiency and sustainability.

C. CDR Analysis for RIES

The loads with demand response capability mentioned in this paper include electricity loads and heat loads, which respond to their own demand based on the energy trading prices set by RIES operators.

Figures 7 and 8 show the operation plans of electricity and heat loads before and after demand response, respectively. As illustrated in Fig. 6, it can be observed that during the 10^{th}-18^{th} hours when the electricity price of RIES operator is high, the operator significantly reduces the fluctuation of the electricity load by interrupting the electricity load and transferring it to the period with low electricity prices, achieving the effect of peak shaving and valley filling. However, it is worth noting that after the demand response, the fluctuation of the heat load is not obvious. This is because the heating

price does not vary much during each time period, and reducing the heat load is not conducive to improving the economic operation of the system.

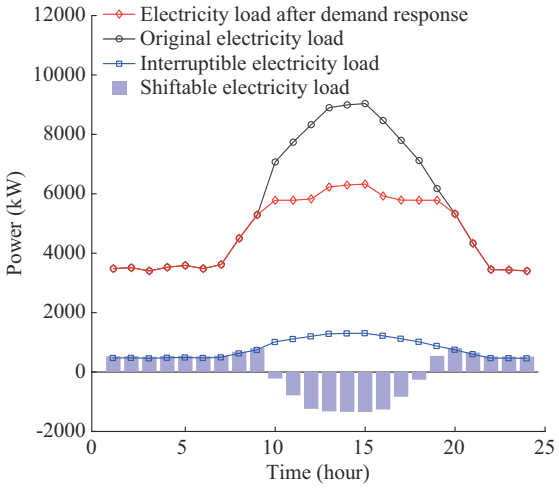

Fig. 7. Operation plans of electricity load before and after demand response.

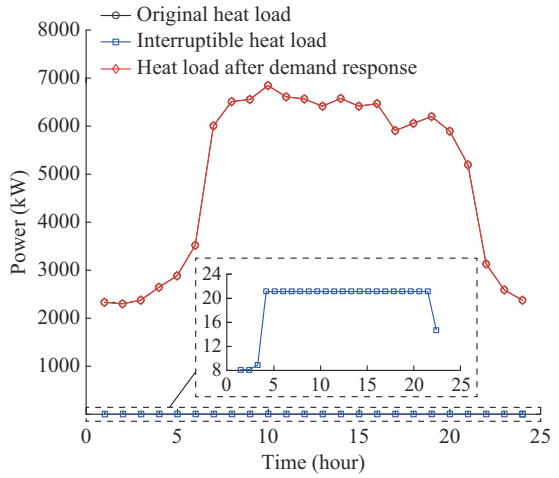

Fig. 8. Operation plans of heat load before and after demand response.

To further illustrate the rationality and feasibility of the proposed CDR scheme in this paper, a comparison is made between this scheme and a scheme that does not consider users' CDR behavior (without a master-slave game relationship), which is denoted as scheme 1.

A comparison of the energy cost and comprehensive benefits of RIES users under different schemes is shown in Table V. It shows that the proposed CDR scheme results in an 8.99% reduction in energy costs for users while significantly increasing their comprehensive benefits by 58.79%. Overall, the introduction of CDR in RIES alleviates the energy supply pressure during peak periods for RIES operators and benefits users by providing economically comfortable energy use, achieving a win-win situation.

D. Optimal Scheduling Results for RIES

This subsection utilizes a sample of 5000 historical wind power generation scenarios from a specific location in China.

TABLE V
COMPARISON OF ENERGY COST AND COMPREHENSIVE BENEFITS OF RIES USERS UNDER DIFFERENT SCHEMES

Scheme	Energy cost (CNY)	Comprehensive benefit (CNY)
1	41892.48	32674.21
Proposed	38123.91	51883.26

The scenarios are further divided into ten discrete cases for analysis. The results of the optimal scheduling from the proposed model are displayed in Fig. 9 and Fig. 10.

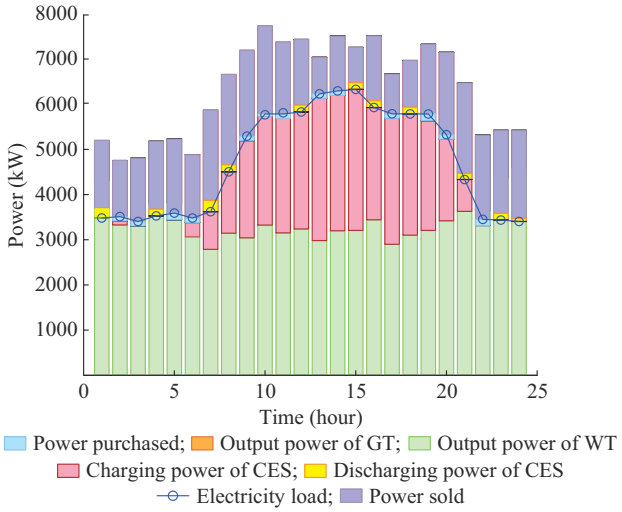

Fig. 9. Optimal electricity supply plan for RIES.

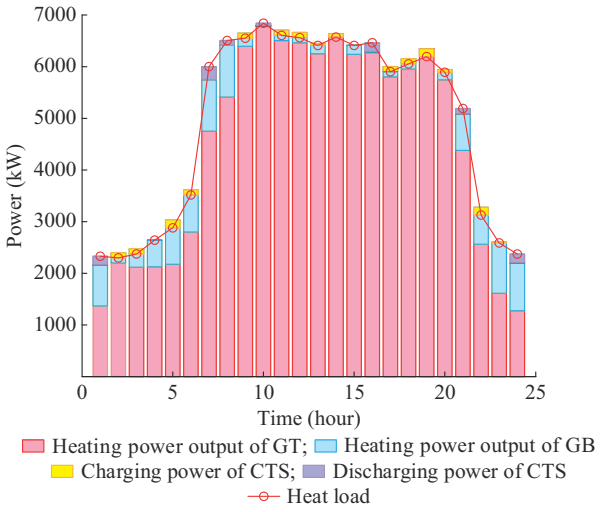

Fig. 10. Optimal heating supply plan for RIES.

1) Optimal Electricity Supply Plan for RIES

In the context of optimizing electricity supply, as illustrated in Fig. 9, the RIES implements a moderate to low level of electricity supply from the 0^{th}-8^{th} hours and 16^{th}-24^{th} hours. These time frames are characterized by abundant wind power resources with minimal fluctuations, sufficiently meeting the majority of the load demand. Furthermore, due to the need for heating power, the GT generates surplus electricity that exceeds the local consumption. Consequently, this

excess electricity is sold to the higher-level grid during these periods, generating revenue and reducing carbon emissions for the RIES.

Additionally, during these periods, operators actively charge the GTs. The stored energy is later discharged and utilized during high-demand periods. This load-shifting strategy effectively manages peaks in electricity consumption, thereby contributing to a more balanced and efficient electricity supply system.

2) Optimal Heating Supply Plan for RIES

Concerning the optimization of heating supply, the heating model in this study incorporates GT and GB. The electricity generated by the GT and WT is used to meet the demand response for electricity loads, while the heat produced simultaneously maintains the heat balance of the system. As depicted in Fig. 10, the heat load supplied by the RIES is lower in the evening and at night but increases significantly during the day time. During the periods from 0^{th}-5^{th} horus and 16^{th}-24^{th} hours, the RIES experiences less pressure in the heating supply, allowing for the utilization of CHS systems to charge heat. This stored heat is then utilized to meet the high-demand periods, thereby reducing the constraints imposed by the heat-to-power ratio of GT and improving the integration rates of wind power. Consequently, this model effectively reduces carbon emissions from the system, promoting a more sustainable and eco-friendly operation.

VI. Conclusion

This study focuses on the integration of multiple stakeholders in the RIES. A TSDRGM based on Stackelberg game theory involving RIES operators and CDR users is proposed. The efficient C&CG algorithm is employed to iteratively solve the master problem and subproblems. The validation of the proposed model leads to the following conclusions.

1) The optimal scheduling strategy presented in this study significantly improves the economic efficiency of system operation through the Stackelberg game process between RIES operators and CDR users, effectively handling different levels of wind power forecast errors. The strategy demonstrates its capability to effectively mitigate uncertainties and risks associated with wind power forecast.

2) The distributionally robust optimization allows for well-balanced trade-offs between the economic performance and the robustness of scheduling plans. It achieves this by flexibly adjusting confidence levels, combining the advantages of stochastic optimization, which reflects expected risks based on historical forecast error data, and strong robustness in robust optimization.

3) The CDR scheme proposed in this paper realizes the demand response of electricity and heat loads within a reasonable range, reducing the user's energy cost by 8.99% and significantly increasing the user's energy satisfaction by 58.79%. This not only alleviates the energy supply pressure of RIES operators during peak periods but also benefits users by providing economically comfortable energy use.

4) The proposed model and strategy hold promise for achieving optimal scheduling in RIESs considering the interests of various stakeholders, and effectively handling uncertainties in energy generation and demand response.

This paper examines energy pricing through a master-slave game without addressing the actual pricing mechanism for optimal energy pricing. Future research should explore more comprehensive optimization configuration schemes to promote the coordinated development of RIESs.

References

[1] J. Wang, H. Zhong, Z. Yang *et al*., "Exploring the trade-offs between electric heating policy and carbon mitigation in China," *Nature Communications*, vol. 11, p. 6054, Nov. 2020.

[2] Q. Meng, J. Xu, F. Luo *et al*., "Collaborative and effective scheduling of integrated energy systems with consideration of carbon restrictions," *IET Generation*, *Transmission & Distribution*, vol. 17, no. 18, pp. 4134-4145, Sept. 2023.

[3] X. Jin, H. Jia, Y. Mu *et al*., "A stackelberg game based optimization method for heterogeneous building aggregations in local energy markets," *IEEE Transactions on Energy Markets*, *Policy and Regulation*, vol. 1, no. 4, pp. 360-372, Dec. 2023.

[4] P. Li, F. Zhang, X. Ma *et al*., "Operation cost optimization method of regional integrated energy system in electricity market environment considering uncertainty," *Journal of Modern Power Systems and Clean Energy*, vol. 11, no. 1, pp. 368-380, Jan. 2023.

[5] Q. Meng, J. Xu, L. Ge *et al*., "Economic optimization operation approach of integrated energy system considering wind power consumption and flexible load regulation," *Journal of Electrical Engineering & Technology*, vol. 19, no. 1, pp. 209-221, Jan. 2024.

[6] L. Ge, Y. Li, J. Yan *et al*., "Short-term load prediction of integrated energy system with wavelet neural network model based on improved particle swarm optimization and chaos optimization algorithm," *Journal of Modern Power Systems and Clean Energy*, vol. 9, no. 6, pp. 1490-1499, Nov. 2021.

[7] Q. Xu, L. Li, X. Chen *et al*., "Optimal economic dispatch of combined cooling, heating and power-type multi-microgrids considering interaction power among microgrids," *IET Smart Grid*, vol. 2, no. 3, pp. 391-398, Sept. 2019.

[8] X. Wang, C. Yang, M. Huang *et al*., "Multi-objective optimization of a gas turbine-based CCHP combined with solar and compressed air energy storage system," *Energy Conversion and Management*, vol. 164, pp. 93-101, May 2018.

[9] S. Bahrami and A. Sheikhi, "From demand response in smart grid toward integrated demand response in smart energy hub," *IEEE Transactions on Smart Grid*, vol. 7, no. 2, pp. 650-658, Aug. 2016.

[10] N. Liu, L. He, X. Yu *et al*., "Multiparty energy management for grid-connected microgrids with heat- and electricity-coupled demand response," *IEEE Transactions on Industrial Informatics*, vol. 14, no. 5, pp. 1887-1897, May 2018.

[11] N. Liu, L. Zhou, C. Wang *et al*., "Heat-electricity coupled peak load shifting for multi-energy industrial parks: a stackelberg game approach," *IEEE Transactions on Sustainable Energy*, vol. 11, no. 3, pp. 1858-1869, Jul. 2020.

[12] J. Chen, B. Qi, Z. Rong *et al*., "Multi-energy coordinated microgrid scheduling with integrated demand response for flexibility improvement," *Energy*, vol. 217, p. 119387, Feb. 2021.

[13] X. Jin, Q. Wu, H. Jia *et al*., "Optimal integration of building heating loads in integrated heating/electricity community energy systems: a bi-level MPC approach," *IEEE Transactions on Sustainable Energy*, vol. 12, no. 3, pp. 1741-1754, Jul. 2021.

[14] M. Sim, D. Bertsimas, and M. Zhang, "Adaptive distributionally robust optimization," *Manage Science*, vol. 65, no. 2, pp. 604-618, Feb. 2019.

[15] Q. Meng, G. Zu, L. Ge *et al*., "Dispatching strategy for low-carbon flexible operation of park-level integrated energy system," *Applied Sciences*, vol. 12, no. 23, p. 12309, Dec. 2022.

[16] Y. Li, F. Bu, J. Gao *et al*., "Optimal dispatch of low-carbon integrated energy system considering nuclear heating and carbon trading," *Journal of Cleaner Production*, vol. 378, p. 134540, Dec. 2022.

[17] J. Wang, L. Chen, Z. Tan *et al*., "Inherent spatiotemporal uncertainty of renewable power in China," *Nature Communications*, vol. 14, no. 1, p. 5379, Sept. 2023.

[18] T. Ding, Q. Yang, Y. Yang *et al*., "A data-driven stochastic reactive power optimization considering uncertainties in active distribution net-

works and decomposition method," *IEEE Transactions on Smart Grid*, vol. 9, no. 5, pp. 4994-5004, Sept. 2018.
[19] Y. Cao, W. Wei, L. Chen *et al*., "Supply inadequacy risk evaluation of stand-alone renewable powered heat-electricity energy systems: a data-driven robust approach," *IEEE Transactions on Industrial Informatics*, vol. 17, no. 3, pp. 1937-1947, Mar. 2021.
[20] W. Fan, L. Ju, Z. Tan *et al*., "Two-stage distributionally robust optimization model of integrated energy system group considering energy sharing and carbon transfer," *Applied Energy*, vol. 331, p. 120426, Feb. 2023.
[21] W. Wang, S. Huang, G. Zhang *et al*., "Optimal operation of an integrated electricity-heat energy system considering flexible resources dispatch for renewable integration," *Journal of Modern Power Systems and Clean Energy*, vol. 9, no. 4, pp. 699-710, Aug. 2021.
[22] H. Zhao, B. Wang, X. Wang *et al*., "Active dynamic aggregation model for distributed integrated energy system as virtual power plant," vol. 8, no. 5, pp. 831-840, Sept. 2020.
[23] W. Zheng and D. Hill, "Distributed real-time dispatch of integrated electricity and heat systems with guaranteed feasibility," *IEEE Transactions on Industrial Informatics*, vol. 18, no. 2, pp. 1175-1185, Feb. 2022.
[24] Y. Li, M. Han, M. Shahidehpour *et al*., "Data-driven distributionally robust scheduling of community integrated energy systems with uncertain renewable generations considering integrated demand response," *Applied Energy*, vol. 335, p. 120749, Apr. 2023.
[25] F. T. Hamzehkolaei, N. Amjady, and B. Bagheri, "A two-stage adaptive robust model for residential micro-CHP expansion planning," *Journal of Modern Power Systems and Clean Energy*, vol. 9, no. 4, pp. 826-836, Aug. 2021.
[26] S. He, H. Gao, H. Tian *et al*., "A two-stage robust optimal allocation model of distributed generation considering capacity curve and real-time price based demand response," *Journal of Modern Power Systems and Clean Energy*, vol. 9, no. 1, pp. 114-127, Jan. 2021.
[27] J. Zhang, M. Cui, Y. He *et al*., "Multi-period two-stage robust optimization of radial distribution system with cables considering time-of-use price," *Journal of Modern Power Systems and Clean Energy*, vol. 11, no. 1, pp. 312-323, Jan. 2023.

Qinglin Meng received the B.S. and M.S. degrees in electrical engineering from Tianjin University, Tianjin, China, in 2003 and 2010, respectively. He is currently the Deputy Division Chief of the Operational Audit Division at the Comprehensive Service Center of State Grid Tianjin Electric Power Company, Tianjin, China. Additionally, he acts as a Postgraduate Supervisor in enterprise at both Tianjin University and Tiangong University, Tianjin, China. His research interests include power distribution system, integrated energy system, power cable technology, and artificial intelligence audit technology.

Xiaolong Jin received the B.S., M.S., and Ph.D. degrees in electrical engineering from Tianjin University, Tianjin, China, in 2012, 2015, and 2018, respectively. He is currently an Associate Professor with the School of Electrical and Information Engineering, Tianjin University. From 2019 to 2022, he was a Postdoc Researcher with the Centre of Electric Power and Energy, Department of Electrical Engineering, Technical University of Denmark, Lyngby, Denmark. From 2017 to 2019, he was a joint Ph.D. student with the School of Engineering, Cardiff University, Cardiff, UK. His main research interests include energy management of multi-energy buildings and their integrations with integrated energy systems, and energy and flexibility market solutions.

Fengzhang Luo received the B.S., M.S., and Ph.D. degrees in electrical engineering from Tianjin University, Tianjin, China, in 2003, 2006, and 2010, respectively. He is currently an Associate Professor with the School of Electrical and Information Engineering, Tianjin University. His main research interests include active distribution system planning and decision-making and artificial intelligence application in power systems.

Zhongguan Wang received the B.S. and Ph.D. degrees in electrical engineering from Tsinghua University, Beijing, China, in 2014 and 2019, respectively. He is currently an Associate Professor with the School of Electrical and Information Engineering, Tianjin University, Tianjin, China. He has been a Visiting Scholar with the School of Applied Engineering Harvard University, Harvard University, Cambridge, USA, in 2018. His current research interests include operation of renewable power generation and energy management of active distribution system.

Sheharyar Hussain received the B.S. degree in electrical power engineering from Fast-National University of Computer and Emerging Sciences, Islamabad, Pakistan, in 2017. He holds two M.S. degrees, one in control science and automation engineering from Shanghai Jiaotong University, Shanghai, China, in 2020, and another in electronic information from Ocean College, Zhejiang University, Zhoushan, China, in 2024. He is currently engaged in research collaboration with Zhejiang University and the University of Hull, Hull, UK. His main research interests include robotics, robust control and optimization, regional integrated energy system, renewable energy, model predictive control, and electro-mechanical machines.